Deriving intertidal topography from SWOT data and Sentinel-2 data

ADVANCING EARTH AND SPACE SCIENCES

Geophysical Research Letters®

RESEARCH LETTER
10.1029/2025GL117329

Special Collection:
Science from the Surface Water and Ocean Topography Satellite Mission

Deriving Intertidal Topography From SWOT Data and Sentinel-2 Data

Mingzhi Sun[1,2], Wei Feng[1,3], Xudong Wang[1], Nan Xu[4], Fukai Peng[1,3], Xiaodong Chen[1], Dechao An[1], Luciana Fenoglio[2], Meng Yang[1,3], and Min Zhong[1,3]

[1]School of Geospatial Engineering and Science, Sun Yat-sen University, Zhuhai, China, [2]Institute of Geodesy and Geoinformation, University of Bonn, Bonn, Germany, [3]Key Laboratory of Comprehensive Observation of Polar Environment (Sun Yat-sen University), Ministry of Education, Zhuhai, China, [4]School of Architecture & Urban Planning, Shenzhen University, Shenzhen, China

Key Points:

- A method was proposed to generate 10 m resolution intertidal topography on the coast of Jiangsu, China, using Surface Water and Ocean Topography (SWOT) and Sentinel-2 data
- The density-based spatial clustering of applications with noise method identifies outliers and filters SWOT observations
- SWOT L2_HR_PIXC data shows high accuracy for intertidal monitoring, with RMSEs of 0.24 m (multi-cycle) and 0.41 m (single-cycle)

Supporting Information:

Supporting Information may be found in the online version of this article.

Correspondence to:

W. Feng,
fengwei@sysu.edu.cn

Citation:

Sun, M., Feng, W., Wang, X., Xu, N., Peng, F., Chen, X., et al. (2025). Deriving intertidal topography from SWOT data and Sentinel-2 data. *Geophysical Research Letters*, *52*, e2025GL117329. https://doi.org/10.1029/2025GL117329

Received 29 MAY 2025
Accepted 22 OCT 2025

Author Contributions:

Conceptualization: Mingzhi Sun, Wei Feng, Fukai Peng
Data curation: Mingzhi Sun, Wei Feng, Xudong Wang, Nan Xu, Meng Yang
Funding acquisition: Wei Feng
Methodology: Mingzhi Sun, Wei Feng, Xudong Wang, Nan Xu, Fukai Peng, Xiaodong Chen, Dechao An, Meng Yang
Project administration: Wei Feng
Resources: Wei Feng

Abstract The Surface Water and Ocean Topography (SWOT) mission, initially designed to observe oceans and inland waters, proves valuable for mapping intertidal flat topography. This study presents a fusion method that integrates freely available SWOT interferometric altimetry data with Sentinel-2 imagery. The density-based spatial clustering of applications with noise algorithm is employed to accurately identify observation data located in the intertidal zone. Intertidal topography with a 10 m resolution were generated from L2_HR_PIXC data collected during SWOT's science phase (July 2023–October 2024) in the intertidal region along the coast of Jiangsu Province, China. These Digital Elevation Models were compared with laser altimetry observations from the ICESat-2. SWOT observations show high accuracy, with RMSEs of 0.24 m (multi-cycle) and 0.41 m (single-cycle), confirming their potential for intertidal monitoring. This study presents a data processing strategy that does not rely on ground-based observations, demonstrating potential for application in a broader range of regions.

Plain Language Summary The Surface Water and Ocean Topography (SWOT) mission, initially designed to study oceans and inland waters, has also proven to be very useful for mapping the shape of the intertidal zone—the land submerged during high tide and exposed during low tide. This study used a combination of freely available satellite images from Sentinel-2 and SWOT to create detailed maps of intertidal topography. The data collected between July 2023 and October 2024, during the scientific phase of the SWOT mission, was used to produce these maps. To verify the accuracy of these maps, we compared them with measurements from a laser altimetry satellite. We find that the data from SWOT is highly accurate and can effectively capture slight changes in the tidal flat areas. This study also indicates that SWOT is not just useful for measuring water levels, but can play a broader role in monitoring and managing coastal areas, making it a valuable tool for environmental studies and coastal protection.

1. Introduction

Intertidal flats, dynamic environments located at the land-sea interface, are characterized by constantly changing landscapes. Regular monitoring of intertidal topography is essential for understanding and managing these areas, which provide critical societal and economic services (Murray et al., 2018). Satellites are currently the most practical tool for mapping intertidal topography at a global scale with consistent updates. The development of space-borne methods for measuring intertidal topography began 30 years ago (Salameh et al., 2019; H. Zhang et al., 2021). One of the most effective approaches is the waterline method, introduced by Mason et al. (1995). This technique involves extracting waterlines from radar or optical images acquired at different tidal stages, assigning elevations to these waterlines using in situ or modeled sea level data, and then interpolating them to create gridded intertidal Digital Elevation Model (DEM). N. Xu et al. (2024) proposed a method for mapping intertidal topography based on flood frequency and Ice, Cloud, and Land Elevation Satellite-2 (ICESat-2) altimetry data. This method relies entirely on satellite data and requires no in situ data, improving the ability to map intertidal topography in many coastal areas. However, both the waterline and inundation frequency methods estimate elevations based on a priori elevation, and the accuracy of the model is limited by the a priori elevation data.

The tidal topography can also be measured directly using interferometric synthetic aperture radar (InSAR) observations (Lee & Ryu, 2017). Single-pass interferometric systems, like the recently launched Surface Water and

Software: Mingzhi Sun, Xudong Wang, Xiaodong Chen, Dechao An
Supervision: Wei Feng, Luciana Fenoglio, Min Zhong
Validation: Mingzhi Sun, Wei Feng, Nan Xu, Xiaodong Chen, Dechao An, Meng Yang
Visualization: Mingzhi Sun, Xiaodong Chen
Writing – original draft: Mingzhi Sun
Writing – review & editing: Mingzhi Sun, Wei Feng, Nan Xu, Fukai Peng, Luciana Fenoglio, Min Zhong

Ocean Topography (SWOT) mission, allow InSAR acquisitions without a temporal baseline (Fu et al., 2024). SWOT's altimeter data thus have substantial potential for coastal and regional geospatial applications (Hwang & Yu, 2024). SWOT is expected to combine both the waterline and direct InSAR methods to generate intertidal DEMs (Salameh et al., 2021). The InSAR method, requiring only a single acquisition at low tide, offers a key advantage over the waterline method (Salameh et al., 2024), which typically needs a series of images spanning multiple tidal cycles—usually 3–4 months of data from SWOT's 21-day science orbit (Salameh et al., 2021). Salameh et al. (2024) were the first to demonstrate the SWOT's ability to accurately measure intertidal topography, generating topography maps for the Bay of Veys in France using the L2_HR_PIXC product, validated against LiDAR data from both the calibration and scientific orbits. Similarly, Shi et al. (2025) modeled intertidal topography along Jiangsu Province's coast using 250 m resolution SWOT data, extracting tidal flat observations from height gradients. However, both studies relied either on global tidal model outputs or on in situ tide gauge records to filter low-tide SWOT passes, whereas this study instead uses SWOT-derived sea surface height (SSH) as a substitute for tidal measurements.

This study presents a method for constructing intertidal topography using satellite data alone. Since SWOT simultaneously observes both sea level and tidal flat elevation, we extract SSH from SWOT data as a substitute for tidal station measurements. The method was validated on the largest tidal flat in Jiangsu Province, China. Sentinel-2 data were used to delineate intertidal boundaries, while density-based clustering methods were used to accurately identify outliers. The accuracy of the SWOT-derived DEM was further evaluated by the ICESat-2 satellite (N. Xu et al., 2022).

2. Methods and Materials

2.1. Study Area and Data

The study area is a typical tidal flat along the coast of Jiangsu Province, China (Figure 1), featuring a series of radial submarine sand ridges on the Yellow Sea seafloor. The largest tidal flat, located on the Chinese continental shelf, stretches approximately 200 km North-South and 90 km East-West, covering over 1,018 km^2 (N. Xu et al., 2022). Over recent decades, there has been a trend of expansion in the area of these tidal flats (Murray et al., 2018; Wang et al., 2019).

The SWOT mission operates in a non-sun-synchronous orbit with a 21-day repeat cycle (20.86455 days) at an altitude of 890.6 km and an inclination angle of 77.6° during its science phase. SWOT operates in two distinct modes: the High Rate (HR) mode, designed for monitoring continental waters and coastal areas, and the Low Rate mode, which provides global coverage, primarily focusing on oceanic waters. The SWOT L2_HR_PIXC 2.0 data set consists of the KaRIn HR point cloud of pixel cloud (PIXC), including geolocated heights, backscatter, geophysical fields, and flags (JPL-D-56411, 2025). The L2_HR_PIXC product is available in 64 × 64 km tile-sized granules, where the term granule in this context represents the downloadable unit of the data product. For further details on the L2_HR_PIXC product, refer to JPL-D-56411 (2025).

The multispectral imagery from Sentinel-2 was employed to delineate the boundaries of tidal flat topography. Sentinel-2, a twin-satellite mission with a 10 m spatial resolution and a 5-day revisit period, has been available since June 2015. The data were processed using the Google Earth Engine (GEE) platform, using the Multi-Spectral Instrument Level-2A data set to calculate inundation frequency (N. Xu et al., 2024). The Sentinel-2 Level-2A Harmonized Surface Reflectance data set (COPERNICUS/S2_SR_HARMONIZED) includes atmospheric and geometric corrections, spectral harmonization between Sentinel-2A and 2B, and resampling to consistent spatial resolutions. Enhanced cloud and shadow masking is provided via the QA60 and MSK_CLOUDS bands for improved quality control in time-series analysis. On 03 April 2024, ICESat-2 passed over the study area on a descending track (Figure 1). ICESat-2 data from the tidal flat region were manually selected to validate the SWOT-derived DEM. A detailed description of ICESat-2 and the process for manually selecting data can be found in Figures S4 and Text S1 in Supporting Information S1. The SWOT and ICESat-2 observations were converted into orthometric heights using the EGM2008 model. This model integrates global area-mean free-air gravity anomalies derived from a 5′ grid, which combines data from terrestrial, altimetric, and airborne gravity measurements. The EGM2008 model extends up to degree and order 2159 (Pavlis et al., 2012). The accuracy of SWOT-derived DEM was assessed by calculating the RMSE and the coefficient of determination (R^2).

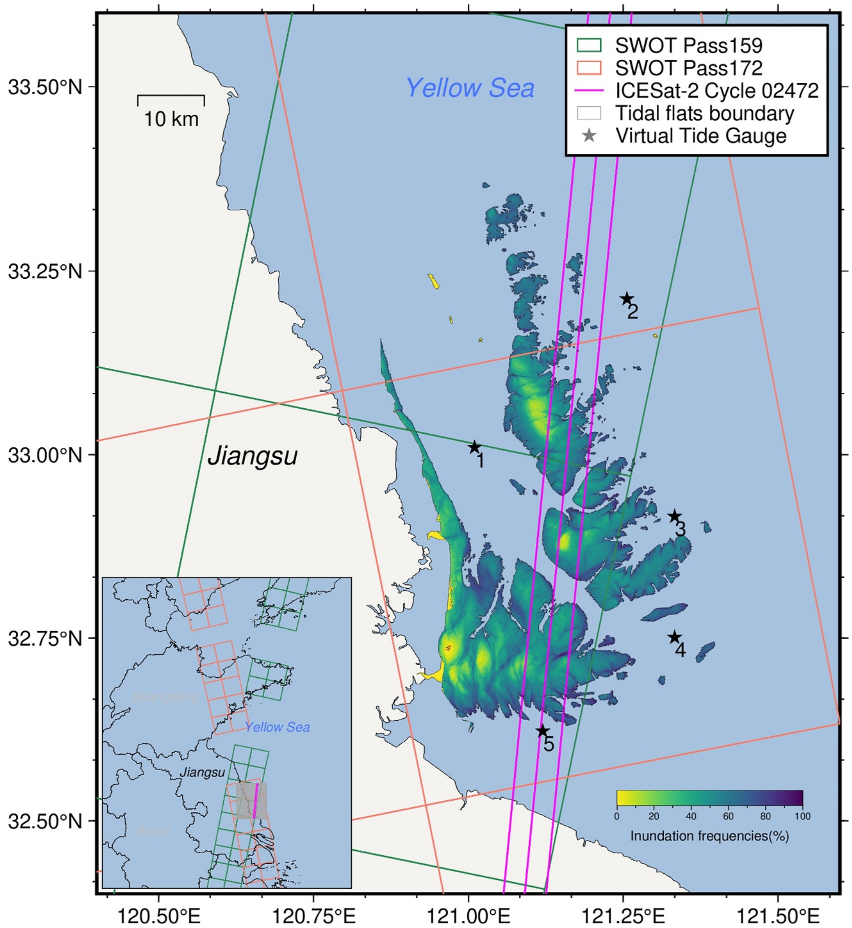

Figure 1. Overview of the tidal flat along the coast of Jiangsu Province, China. Further zoom-in shows the ICESat-2 and Surface Water and Ocean Topography (SWOT) tracks. Colors represent inundation frequency, derived from Sentinel-2 data, which is used to define the intertidal boundary. Five virtual tide gauge stations will be used to obtain sea surface height during satellite overflights. Data from the ICESat-2 satellite, scheduled to fly over the region on 03 April 2024, will be used to assess the accuracy of the SWOT-derived Digital Elevation Model.

2.2. Method and Workflow

This study presents a three-step approach for deriving intertidal topography using satellite data, as illustrated in Figure 2. Step 1 involves creating an inundation frequency map from a time series of Sentinel-2 imagery, which is used to delineate the intertidal boundary. In Step 2, the inundation frequency data are integrated with SWOT observations from each tile, providing the necessary inputs for the construction of the DEMs. Step 3 uses orthometric heights to generate the final tidal flat topographic map by combining all the data processed in Step 2. The resulting topography map is produced at a spatial resolution of 10 m, consistent with the resolution of the Sentinel-2 images.

In the first step, Sentinel-2 data were used to map the intertidal boundaries. The QA60 band (a quality assessment band in Sentinel-2 imagery that flags clouds, cirrus clouds, and shadows at 60 m spatial resolution) of each image was utilized to create a clear observation map, where clear pixels were assigned a value of 1, and clouds and shadows were assigned 0. For the clear pixels, the Normalized Difference Vegetation Index (NDVI) was applied to enhance the contrast between land and water (McFeeters, 1996). NDVI was selected over the Normalized Difference Water Index (NDWI) due to its superior ability to distinguish between various land cover types (such as bare soil, sand, and wetlands) and water bodies in tidal flat environments. While NDWI performs well in identifying clear water, its effectiveness decreases in turbid conditions. In contrast, NDVI enhances the contrast between land and water, making it particularly suitable for delineating tidal flat distributions in dynamic coastal

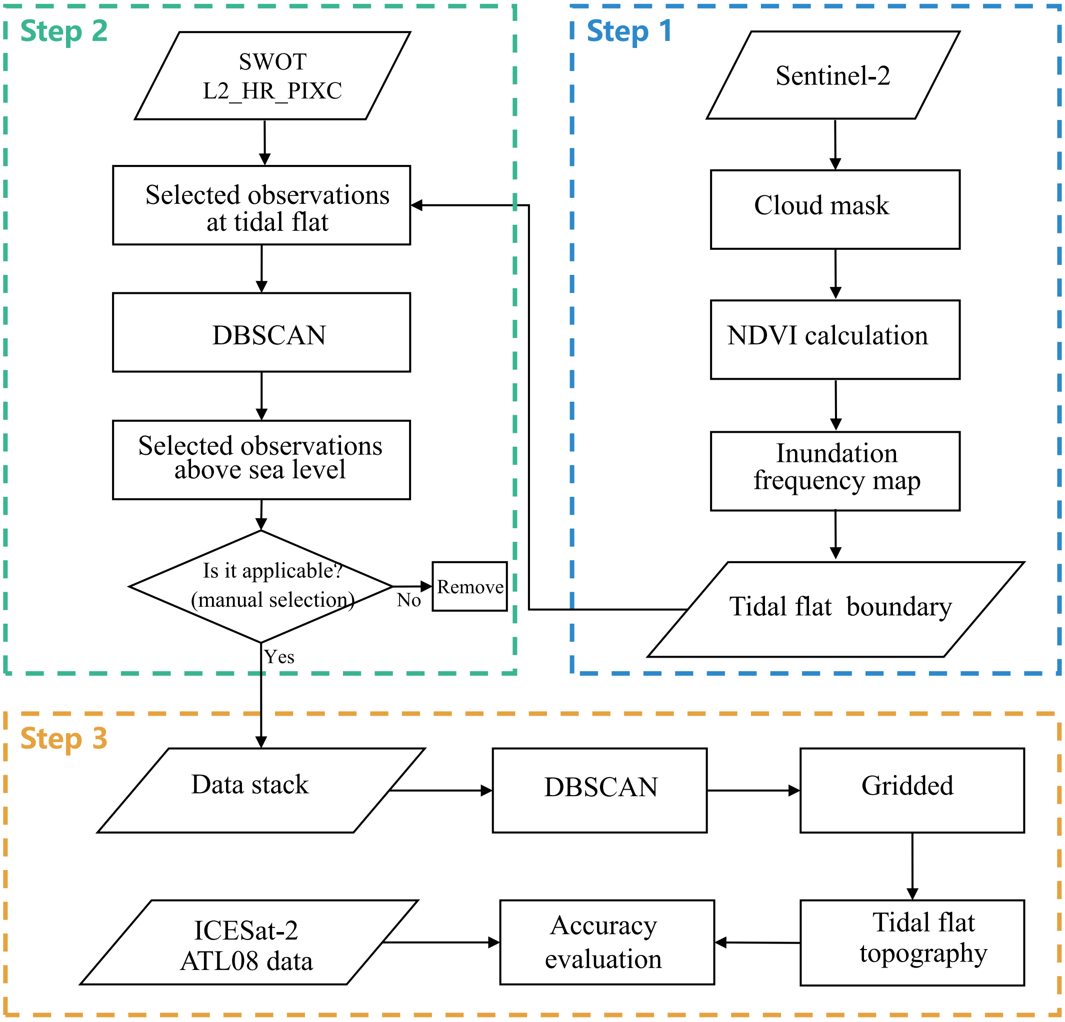

Figure 2. Flow chart for deriving intertidal topography using Sentinel-2 images and Surface Water and Ocean Topography pixel cloud observations. Outliers are identified using the density-based spatial clustering of applications with noise clustering algorithm.

zones. Calculated using Near Infrared (NIR) and red bands, which are minimally influenced by water turbidity, NDVI values range from −1 to 1. The NDVI is calculated as follows:

$$\mathrm{NDVI} = \frac{\rho_{\mathrm{nir}} - \rho_{\mathrm{red}}}{\rho_{\mathrm{nir}} + \rho_{\mathrm{red}}} \tag{1}$$

where ρ_{nir} is near infrared wave band reflectance with a central wavelength of 835.1 nm (S2 A)/833 nm (S2B), ρ_{red} is red band reflectance with a central wavelength of 664.5 nm (S2 A)/665 nm (S2B).

This NDVI was then used to create a 10 × 10 m waterline map, distinguishing between exposed tidal flats (value = 1) and seawater (value = 0) (H. Xu, 2007). A clear observation map was generated by stacking all available Sentinel-2 images from the study period, along with a map of exposed tidal flat counts. The tidal flat inundation frequency map was derived by dividing the exposed tidal flat map by the clear observation map, producing a percentage value in integer format. Level-1C (L1C) top-of-atmosphere reflectance data sets, available via the GEE, were used in this study. A threshold inundation frequency range of 20%–80% was applied, with pixels in this range classified as tidal flats (N. Xu et al., 2024). Despite thresholding, the tidal flat mask contained scattered pixels and gaps. These gaps were filled and scattered pixels removed using Quantum Geographic Information System, after which the tidal flat boundary was generated.

In the second step, SWOT data were processed individually for each tile. The heights observed by SWOT can be expressed as (JPL-D-56411, 2025):

$$Height = Range + Corr\_ion + Corr\_tro + Corr\_tide + Height\_cor\_xover \tag{2}$$

$$Orthometric\_height = Height + Geoid\_EGM2008 \tag{3}$$

where the *Height* of each pixel is determined by the 3D geolocation of the processed KaRIn measurement. Heights are given relative to the reference ellipsoid and corrected for instrument calibration, signal propagation delays due to the ionosphere (*Corr_ion*), and the dry and wet components of the troposphere (*Corr_tro*), as well as crossover calibration (*Height_cor_xover*). *Corr_tide* contains polar tide and solid tide corrections. A geoid is provided, allowing for the calculation of orthometric heights with respect to the EGM2008. The mask generated in the first step was used for the initial selection of SWOT observations. However, the filtered data contained significant noise, necessitating further processing through clustering analysis.

The filtered data from each pass were clustered using the density-based spatial clustering of applications with noise (DBSCAN), a popular unsupervised clustering algorithm, particularly effective for handling irregularly shaped data with noise (Ester et al., 1996). The algorithm relies on two key parameters: epsilon (*Eps*) and Minimum samples (*min_samples*), which control the density and size of the neighborhood around data points, respectively. The *Eps* defines the maximum distance threshold for a point's neighborhood; if the distance between two points is less than this threshold, they are considered part of the same cluster. The *min_samples* specifies the minimum number of neighboring points required to form a cluster. Points with sufficient neighboring points are classified as core points, and their surrounding points are assigned to the same cluster. In this study, *Eps* was set to 0.1 and *min_samples* to 60, meaning that each data point must have at least 60 neighboring points within a radius of 0.1 to be included in a cluster; otherwise, it is considered noise. Before applying DBSCAN, the input data are standardized to a standard normal distribution with a mean of 0 and a variance of 1.

During SWOT overpasses, inundated areas are excluded from topographic analysis, but accurately removing interference during partial inundation of the intertidal zone is challenging. To address this, five virtual tide gauge stations (Figure 1) were set up near the intertidal zone to obtain SSHs directly from SWOT data. Observations above sea level, representing exposed intertidal topography, were extracted using these stations. The stations were evenly distributed across the tidal flat area, and pixels within a 1.5 km radius were used to calculate average SSHs ("Selected observations above sea level" in Step 2). While adding more stations improves accuracy, it increases the processing workload. Therefore, five stations were used, with stations 1 and 5 applied to both passes 159 and 172. In step three, valid observations were stacked, clustered with DBSCAN, and averaged within 10-m grids to generate the DEMs.

Finally, the accuracy was assessed using 1,140 ICESat-2 ATL08 measurements selected from the intertidal zone to evaluate the SWOT-derived DEM. Additionally, N. Xu et al. (2024) derived an intertidal DEM for this region using inundation frequencies (inundation-based DEMs), which were also used to assess the accuracy of the SWOT-derived DEM. To explore the potential of using a single data cycle for intertidal topography, data from cycle 16 (June 2024), during a low sea level event when most mudflats were exposed and data quality was optimal, were selected. The 61-day interval between this cycle and the ICESat-2 validation data enabled effective comparative analysis.

3. Results and Discussion

3.1. Tidal Flat Topography

Using the data from cycle03pass159 as an example, Figures 3a–3c shows the data processing workflow of Step 2. First, the PIXC observations from pass159 over the tidal flat were filtered (Figure 3a) and processed using DBSCAN. The algorithm identified 382,065 outliers (10.44% of the input data), leaving 3,177,109 valid observations (Figure 3b). The "spots" in the white boxes of Figure 3a were removed as outliers, demonstrating the effectiveness of the DBSCAN method.

Since SWOT observations near the intertidal edge could include sea surface signals, pass 159 extracted SSHs at the time of overflight using three virtual tide gauge stations (1, 2, and 5). Observations above the SSHs (−1.73,

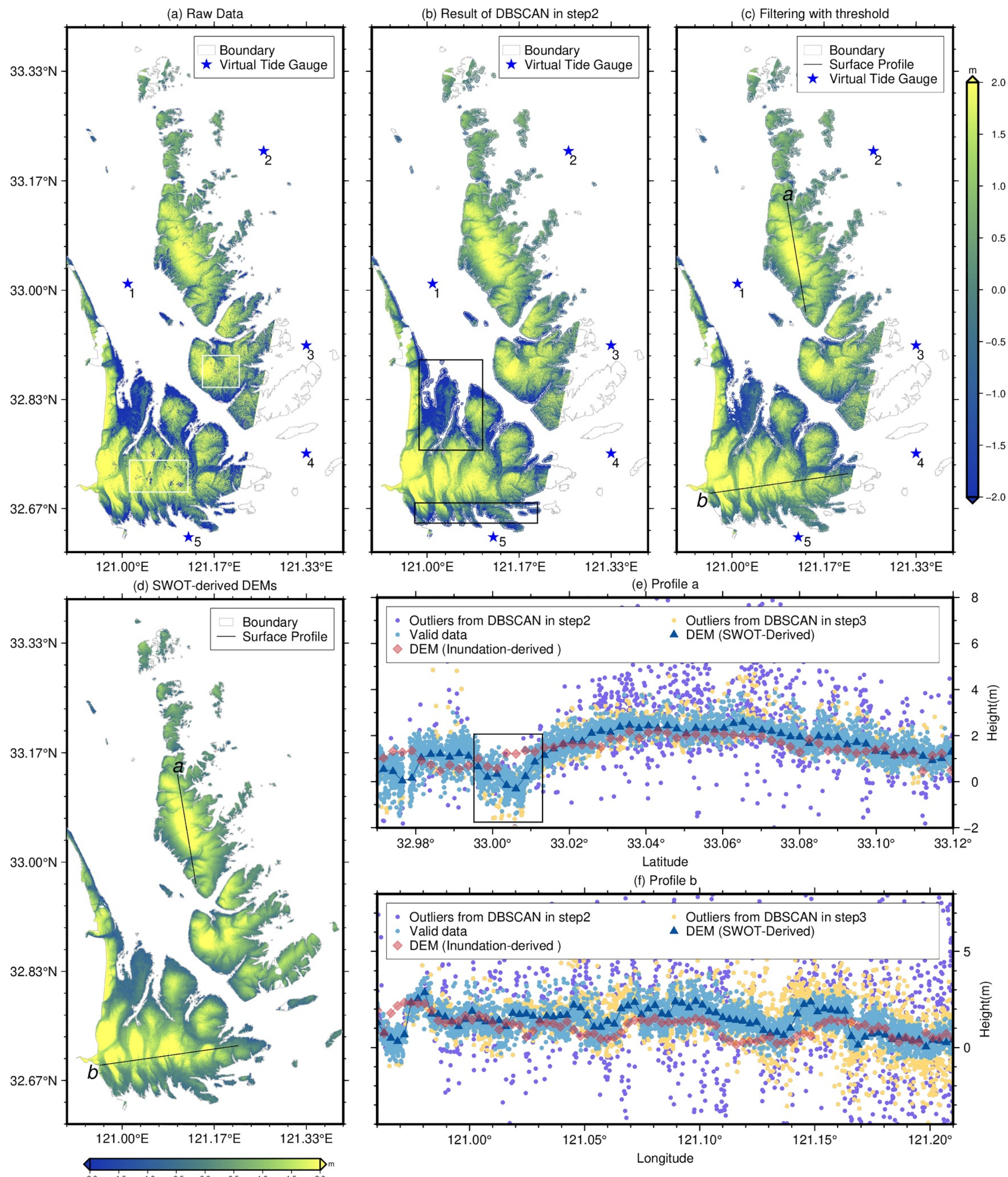

Figure 3. (a–c) Pass 159 of cycle03 is used as an example to demonstrate the data processing for density-based spatial clustering of applications with noise and virtual tide gauge station threshold screening (Step 2, Figure 2). (d) Surface Water and Ocean Topography (SWOT)-derived Digital Elevation Model (DEM) and panels (e, f) illustrate the process of pixel cloud outlier detection along profile lines (a, b). The SWOT-derived DEM were interpolated to the blue triangles, while the red diamonds represent the data from N. Xu et al. (2024).

−0.60, and −1.29 m for stations 1, 2, and 5, respectively) were retained, while those below were discarded. This process removed 303,055 outliers, resulting in 2,874,054 valid data points (Figure 3c). As indicated by the black boxes in Figure 3b, many observations at the edge of the intertidal (dark blue) were removed, yielding smoother remaining data. For pass 172, SSHs will be derived from three nearby virtual tide gauge stations (1, 3, and 4). After initial processing, 15 useful tiles were selected (Figures S2 and S3 in Supporting Information S1) for the DEM construction.

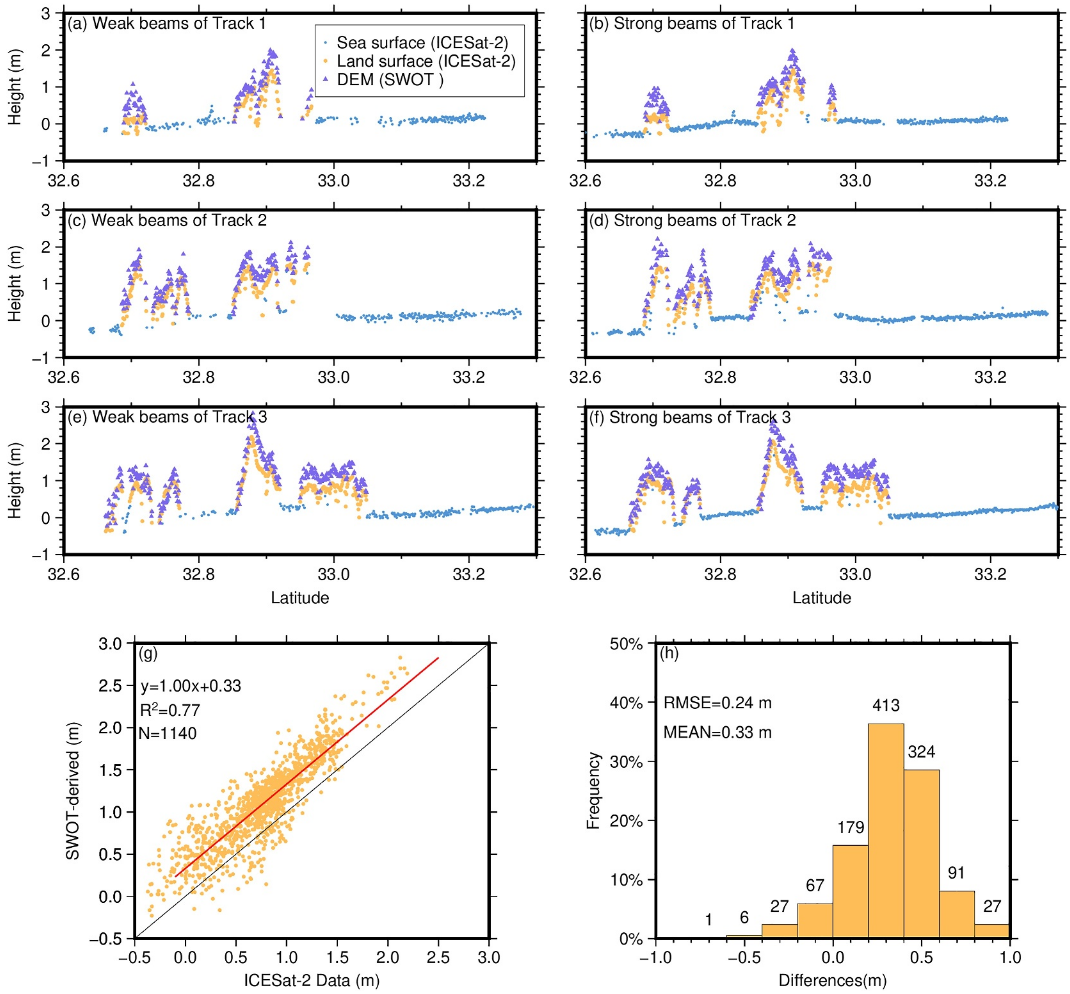

Figure 4. (a–f) The classification of Ice, Cloud, and Land Elevation Satellite-2 (ICESat-2) points was performed manually. (g) Validation of the elevations from our results and ICESat-2 data, (h) along with the normal distribution of their differences.

Two profile lines were established for comparison. Profile (a) extends from 121.13°E, 32.96°N to 121.10°E, 33.13°N, while Profile (b) starts at 120.69°E, 32.69°N and ends at 121.25°E, 32.72°N (both shown in Figure 3d). The PIXC data within 5-m buffers along these profiles are presented in Figures 3e and 3f. Through the DBSCAN processing, most outliers (purple dots) were identified during the secondary clustering phase, with additional marginal outliers (yellow dots) detected in the third step.

The SSHs obtained from virtual tide gauge stations during the SWOT overflights are presented in Table S1 in Supporting Information S1 and served as selection thresholds for valid observations. Prior to threshold application, we performed manual quality control to exclude tiles with complete intertidal submergence or poor-quality data. This process yielded 15 qualified tiles for subsequent analysis.

A total of 15 tiles (~26 million observations) were stacked. The stacked data were then processed using the DBSCAN algorithm (Figure 2, step 3), resulting in the removal of ~2.90 million outliers. The remaining ~23.2 million observations were used to generate gridded DEMs. We first created a 10 m resolution grid and then calculated the mean within each gridcell. The final DEMs are shown in Figure 3d.

3.2. Accuracy of SWOT-Derived DEMs

In Figures 4a–4f, the laser points are shown as surface points (with noise) along the track, and the sea surface points, or noise points, are clearly distinguished from the intertidal. As shown in Figures 4g and 4h, the difference between the data sets follows a normal distribution, with an RMSE of 0.24 m. But a systematic bias of approximately 0.33 m is observed. Although tidal corrections were considered during the data processing, the discrepancy may be due to inaccuracies in the nearshore tidal model or differences between the models used.

The red diamond and blue triangles in Figures 3e and 3f represent the inundation-derived and SWOT-derived DEMs, respectively. The RMSEs for the DEMs along the profiles (a) and (b) are 0.52 and 0.67 m, respectively. The largest discrepancies are found in the tidal creeks, which may be attributed to the differing acquisition dates of the SWOT and ICESat-2 data. Changes in tidal flat topography over time are influenced by coastal morphology, sediment dynamics, and hydrodynamic conditions (Chen et al., 2020). N. Xu et al. (2024) reported an accuracy of 0.49 m for their inundation-based DEM, validated against ICESat-2 data. In comparison, our method outperforms theirs in accuracy, while also offering greater simplicity, efficiency, and significant potential for global application.

The number of observations and the standard deviation (STD) within each gridcell were calculated, as shown in Figures S3a and S3b in Supporting Information S1. It was observed that fewer observations were recorded at the edges of the intertidal zone. Gridcells with higher standard deviations, indicating poorer data quality, are primarily located in tidal channel areas. The terrain slope, shown in Figure S3c in Supporting Information S1, does not exhibit a significant relationship with the spatial distribution of STD. The slope across the entire study area is less than 1°, indicating a flat that is well-suited for SWOT's interferometric mode, which benefits from a small angle of incidence (Salameh et al., 2024). The spatial distribution of these characteristics aligns with the track distribution of pass172, suggesting that future studies should explore alternative PIXC fusion algorithms for constructing more robust results. However, the SWOT-derived DEMs contain some null values due to missing data in approximately 1.30% of the grid. These voids will be filled with more SWOT observations being collected. Lidar point cloud processing methods (W. Zhang et al., 2016) could potentially be used to filter observations located in the tidal flats, however further experiments are needed in the future.

The RMSE of the SWOT-derived DEM from a single cycle was 0.41 m, as shown in Figures S5 and S6 in Supporting Information S1. The accuracy of the DEM derived from one cycle is comparable to that of the waterline and inundation frequency methods, demonstrating that SWOT can effectively monitor intertidal topographic changes. However, data quality varies over different cycles, and more refined processing strategies are needed for more accurate detection of intertidal changes. Additionally, tidal flat changes occur rapidly, with noticeable movement of tidal channels within just 3 months (Shi et al., 2025).

4. Conclusions

The SWOT mission enables continuous spatiotemporal monitoring of sea and inland water. We propose a satellite-only method to derive intertidal topography by fusing SWOT L2_HR_PIXC products and Sentinel-2 imagery, requiring no in situ data. The method was validated over Jiangsu Province's largest intertidal zone (>1,018 km^2).

This study proposes a three-step method for generating tidal flat topography. First, an inundation frequency map derived from Sentinel-2 imagery delineates the intertidal boundary. Second, the DBSCAN clustering algorithm and virtual tide gauge data filter observations for DEM construction. Observations within the vicinity of the virtual tide gauges, classified as water, were removed, and the remaining intertidal observations were processed using the density-based clustering method. Finally, orthometric heights integration produces a 10 m resolution DEM, matching Sentinel-2's resolution. Validation against ICESat-2 data showed high accuracy, with RMSEs of 0.24 m (multi-cycle) and 0.41 m (single-cycle). The single-cycle performance confirms SWOT's potential for monitoring intertidal topographic changes. However, this method relies on SWOT data from low tide periods, meaning not all cycles can be used to construct the DEM. More data and refined processing strategies are needed for monitoring tidal flat changes. Additionally, this clustering method may not be suitable for smaller tidal flats, requiring further experimentation in the future.

Conflict of Interest

The authors declare no conflicts of interest relevant to this study.

Data Availability Statement

All data sets supporting the findings of this study are publicly available. The SWOT Level-2 High-Rate Mode Pixel Cloud (L2_HR_PIXC) product can be accessed through https://hydroweb.next.theia-land.fr/ and https://search.earthdata.nasa.gov/. The Google Earth Engine (GEE) codes used in this study are freely available at https://code.earthengine.google.com/c16d365cb513b92ce4efd205fa886c36?noload=true. The ICESat-2 ATL08 data used for validation in this study are accessible at Neuenschwander et al. (2020). All the data and code (GEE and Python) used in this study are also available at Figshare (Sun, 2025).

Acknowledgments

This study was supported by the National Key Research and Development Program, China (Grant 2024YFC2813500) and Fundamental Research Funds for the Central Universities, Sun Yat-sen University (Grants 24xkjc027 and 23xkjc012). The authors gratefully acknowledge the financial support from the China Scholarship Council (Grant 202406380200).

References

Chen, X., Yu, S., Chen, J., Zhang, C., Dai, W., & Zhang, Q. (2020). Environmental impact of large-scale tidal flats reclamation in Jiangsu, China. *Journal of Coastal Research*, *95*(SI), 315–319. https://doi.org/10.2112/SI95-061.1

Ester, M., Kriegel, H.-P., Sander, J., & Xu, X. (1996). A density-based algorithm for discovering clusters in large spatial databases with noise. In *KDD 96: Proceedings of the second international conference on knowledge discovery and data mining* (pp. 226–231). AAAI Press.

Fu, L.-L., Pavelsky, T., Cretaux, J., Morrow, R., Farrar, J. T., Vaze, P., et al. (2024). The surface water and ocean topography mission: A breakthrough in radar remote sensing of the ocean and land surface water. *Geophysical Research Letters*, *51*(4), e2023GL107652. https://doi.org/10.1029/2023gl107652

Hwang, C., & Yu, D. (2024). Transforming coastal mapping from space. *Science*, *386*(6727), 1222–1223. https://doi.org/10.1126/science.adu0697

JPL-D-56411. (2025). SWOT product description document: Level 2 KaRIn high rate water mask pixel cloud (L2_HR_PIXC) data product. In *Jet propulsion laboratory internal document*.

Lee, S.-K., & Ryu, J.-H. (2017). High-accuracy tidal flat digital elevation model construction using TanDEM-X science phase data. *IEEE Journal of Selected Topics in Applied Earth Observations and Remote Sensing*, *10*(6), 2713–2724. https://doi.org/10.1109/JSTARS.2017.2656629

Mason, D. C., Davenport, I. J., Robinson, G. J., Flather, R. A., & McCartney, B. S. (1995). Construction of an inter-tidal digital elevation model by the 'Water-Line' method. *Geophysical Research Letters*, *22*(23), 3187–3190. https://doi.org/10.1029/95GL03168

McFeeters, S. K. (1996). The use of the normalized difference water index (NDWI) in the delineation of open water features. *International Journal of Remote Sensing*, *17*(7), 1425–1432. https://doi.org/10.1080/01431169608948714

Murray, N. J., Phinn, S. R., DeWitt, M., Ferrari, R., Johnston, R., Lyons, M. B., et al. (2018). The global distribution and trajectory of tidal flats. *Nature*, *565*(7738), 222–225. https://doi.org/10.1038/s41586-018-0805-8

Neuenschwander, A., Pitts, K., Jelley, B., Robbins, J., Klotz, B., Popescu, S., et al. (2020). ATLAS/ICESat-2 L3A land and vegetation height (ATL08, version 3) [Dataset]. *NASA National Snow and Ice Data Center Distributed Active Archive Center*. https://doi.org/10.5067/ATLAS/ATL08.003

Pavlis, N. K., Holmes, S. A., Kenyon, S. C., & Factor, J. K. (2012). The development and evaluation of the Earth gravitational model 2008 (EGM2008). *Journal of Geophysical Research*, *117*(B4), B04406. https://doi.org/10.1029/2011jb008916

Salameh, E., Desroches, D., Deloffre, J., Fjørtoft, R., Mendoza, E. T., Turki, I., et al. (2024). Evaluating SWOT's interferometric capabilities for mapping intertidal topography. *Remote Sensing of Environment*, *314*, 114401. https://doi.org/10.1016/j.rse.2024.114401

Salameh, E., Frappart, F., Almar, R., Baptista, P., Heygster, G., Lubac, B., et al. (2019). Monitoring beach topography and nearshore bathymetry using spaceborne remote sensing: A review. *Remote Sensing*, *11*(19), 2212. https://doi.org/10.3390/rs11192212

Salameh, E., Frappart, F., Desroches, D., Turki, I., Carbonne, D., & Laignel, B. (2021). Monitoring intertidal topography using the future SWOT (surface water and ocean topography) mission. *Remote Sensing Applications: Society and Environment*, *23*, 100578. https://doi.org/10.1016/j.rsase.2021.100578

Shi, H., Jia, D., He, X., Andersen, O. B., & Zheng, X. (2025). SWOT-based intertidal digital elevation model extraction and spatiotemporal variation assessment. *Remote Sensing*, *17*(9), 1516. https://doi.org/10.3390/rs17091516

Sun, M. (2025). Code and data - Deriving intertidal topography from SWOT data and Sentinel-2 data (version 2) [Collection]. *Figshare*. https://doi.org/10.6084/m9.figshare.30005338

Wang, Y., Liu, Y., Jin, S., Sun, C., & Wei, X. (2019). Evolution of the topography of tidal flats and sandbanks along the Jiangsu Coast from 1973 to 2016 observed from satellites. *ISPRS Journal of Photogrammetry and Remote Sensing*, *150*, 27–43. https://doi.org/10.1016/j.isprsjprs.2019.02.001

Xu, H. (2007). Modification of normalised difference water index (NDWI) to enhance open water features in remotely sensed imagery. *International Journal of Remote Sensing*, *27*(14), 3025–3033. https://doi.org/10.1080/01431160600589179

Xu, N., Ma, Y., Yang, J., Wang, X. H., Wang, Y., & Xu, R. (2022). Deriving tidal flat topography using ICESat-2 laser altimetry and Sentinel-2 imagery. *Geophysical Research Letters*, *49*(2), e2021GL096813. https://doi.org/10.1029/2021gl096813

Xu, N., Wang, L., Xu, H., Ma, Y., Li, Y., & Wang, X. H. (2024). Deriving accurate intertidal topography for sandy beaches using ICESat-2 data and Sentinel-2 imagery. *Journal of Remote Sensing*, *4*, 0305. https://doi.org/10.34133/remotesensing.0305

Zhang, H., Hu, L., Zhang, D., Zhou, Y., Ma, Y., Wang, X. H., et al. (2021). A method to derive tidal flat topography in Nantong, China using MODIS data and tidal levels. *Canadian Journal of Remote Sensing*, *47*(1), 17–32. https://doi.org/10.1080/07038992.2021.1879632

Zhang, W., Qi, J., Wan, P., Wang, H., Xie, D., Wang, X., & Yan, G. (2016). An easy-to-use airborne LiDAR data filtering method based on cloth simulation. *Remote Sensing*, *8*(6), 501. https://doi.org/10.3390/rs8060501